

3-D modelling the electric field due to ocean tidal flow and comparison with observations

Alexei Kuvshinov,^{1,2} Andreas Junge,³ and Hisashi Utada⁴

Received 31 October 2005; revised 7 February 2006; accepted 14 February 2006; published 28 March 2006.

[1] The tidal motion of the ocean water through the ambient magnetic field, generates secondary electric field. This motionally induced electric field can be detected in the sea or inland and has a potential for electrical soundings of the Earth. A first goal of the paper is to gain an understanding of the global distribution of the electric signal due to tidal ocean flow. We simulate the electric signals for two tidal constituents - lunar semidiurnal (M2) and diurnal (O1) tides. We assume a realistic Earth's conductivity model with a surface thin shell and 1-D mantle underneath. Simulations demonstrate that in some coastal regions the amplitudes of the electric field can reach 100 mV/km and 10 mV/km for M2 and O1 tides respectively. The changes of lithosphere resistance produce detectable changes in the tidal electric signals. We show that our predictions are in a good agreement with observations. **Citation:** Kuvshinov, A., A. Junge, and H. Utada (2006), 3-D modelling the electric field due to ocean tidal flow and comparison with observations, *Geophys. Res. Lett.*, 33, L06314, doi:10.1029/2005GL025043.

1. Introduction

[2] As the electrically conducting water in the oceans moves in the ambient magnetic field of the Earth, it induces secondary electric and magnetic fields. The EM effects from two types of the ocean flow are mainly studied so far - from steady circulation and from periodic tides. Numerous simulations of the electric and/or magnetic fields have been already made for realistic ocean circulation models [Stephenson and Bryan, 1992; Flosadottir *et al.*, 1997; Palshin *et al.*, 1999; Tyler *et al.*, 1999; Vivier *et al.*, 2004; Manoj *et al.*, 2006] investigating, in particular, a possibility to identify water transport across the straits/open oceans, and detection of the ocean flow variability by EM measurements. As for the tides only magnetic effects have been numerically estimated and analysed until now [Tyler *et al.*, 2003; Maus and Kuvshinov, 2004; Kuvshinov and Olsen, 2005]. The main goal of these model studies was to predict tidal signals in observatory and satellite magnetic fields.

[3] Along with the detection of tidal signals in the magnetic field, many authors [Rooney, 1938; Harvey *et*

al., 1977; Junge, 1988] observed signals from oceanic tides in inland electric field. These signals are also clearly identified in the voltages that are measured with the use of submarine cables [Duffus and Fowler, 1974; Fujii and Utada, 2000]. But so far the work on the subject was confined by experimental observations of the phenomena and no quantitative prediction of the tidal electric fields has been done yet.

[4] This paper presents the results of simulations of the electric field induced within a given conductivity model of the Earth by realistic tidal flows. The primary objectives of the simulations are: 1) to understand the global pattern of the electric fields due to O1 and M2 tides, 2) to investigate the dependence of the tidal electric field and cable voltages on the changes of lithospheric resistance, and 3) to compare our predictions with existing experimental results.

2. Prediction of Tidal Ocean Flow Electric Signal

[5] To predict the electric fields due to the tidal ocean flow, we adopt the numerical solution described by Kuvshinov *et al.* [2002, 2005]. The solution allows simulating the EM fields, excited by some extraneous current, \mathbf{j}^{ext} , in three-dimensional (3-D) spherical models of electric conductivity. Note that in our problem statement, the 3-D model consists of a surface spherical shell of conductance $S(\vartheta, \varphi)$ underlain by radially symmetric conductor, and \mathbf{j}^{ext} degenerates to the sheet current density, \mathbf{J}_τ^{ext} , which is calculated as

$$\mathbf{J}_\tau^{ext} = \sigma_w (\mathbf{U} \times \mathbf{e}_r B_r^m), \quad (1)$$

where $\sigma_w = 3.2$ S/m is the mean sea water conductivity, \mathbf{U} is the depth integrated velocity due to tidal oscillations (Figures 1a–1d) taken from TPXO6.1 global tidal model [Erofeeva and Egbert, 2002], \mathbf{e}_r is the outward unit vector and B_r^m is the radial component of the main magnetic field derived from a model IGRF 2000 (Figure 1f). All the simulations are made on a mesh with a spatial resolution of $1^\circ \times 1^\circ$. The shell conductance $S(\vartheta, \varphi)$ accounts for contribution from the sea water and from the sediments (Figure 1e). The conductance of the ocean layer is derived from the global $5' \times 5'$ NGDC/NOAA's ETOPO bathymetry, multiplying the water depth by σ_w . The conductance of the sediments is calculated from the global sediment thickness given by the $1^\circ \times 1^\circ$ map of Laske and Masters [1997]. For the underlying spherical (1-D) conductor we adopt the Earth's model of Utada *et al.* [2003]. In the course of our model calculations we shall vary the resistance, R , of a 100 km lithosphere (here the resistance

¹Danish National Space Center, Copenhagen, Denmark.

²On leave Institute of Terrestrial Magnetism, Ionosphere and Radio-wave Propagation, Russian Academy of Sciences, Troitsk, Russia.

³Institute of Meteorology and Geophysics, University of Frankfurt am Main, Frankfurt am Main, Germany.

⁴Ocean Hemisphere Research Center, Earthquake Research Institute, University of Tokyo, Tokyo, Japan.

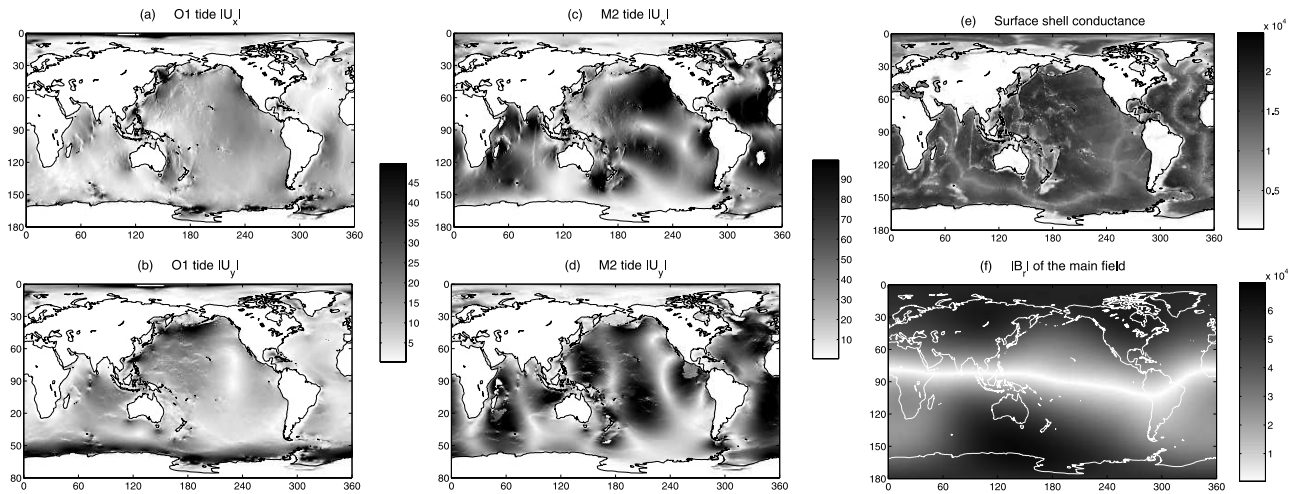


Figure 1. (a)–(d) Amplitudes of depth integrated velocities (m^2/s) of O1 and M2 tides (U_x and U_y are respective south-north and west-east components). (e)–(f) The shell conductance (S) and absolute value of radial component of the main magnetic field (nT).

is a product of the resistivity by the thickness of the lithosphere).

3. Global Pattern of Tidal Electric Fields

[6] Figures 2a–2d present global maps of electric fields due to O1 ($T = 25.81924$ h) and M2 ($T = 12.42059$ h) tides. The O1 and M2 are chosen among others, since they are known as predominantly oceanic tides. For these series of calculations the lithosphere resistance was taken as $10^9 \Omega m^2$. Note, that both velocity and electric field are periodic signals, and so they have in-phase and quadrature parts. But, in order to reduce a number of plots, hereinafter we present only the amplitudes of the signals. It is seen from the figures that sharp contrasts in surface conductance at sea-land contacts (see Figure 1e) produce abrupt enhancement of electric fields on the coasts. Also, as it is expected, maxima of electric field amplitudes in the oceans (that are, however, much less than the coastal signals) follow maxima of

amplitudes of depth-integrated velocities (see Figures 1a–1d). In accordance with the geometry of exciting current (which, in particular, is governed by radial component of the main magnetic field; see Figure 1f and equation (1)), the signals are negligible at the dip equator and increase to the magnetic poles. The largest amplitudes of O1 tide electric field (about 10 mV/km) are predicted at the coast of Antarctica (near the $170^\circ E$), maximum amplitudes of the M2 tide electric field (about 100 mV/km) - on the north-east coast of Canada. Except these ultimate zones there are many coastal regions where one can expect to detect tidal signals. As an example, for the M2 tide these regions are northern Europe, Kamchatka, Japan, western coast of North America, New Zealand, coastal zones of Australia and South Africa.

[7] Figures 2e–2f demonstrate the M2 tide electric field for the model with less resistive lithosphere ($R = 10^7 \Omega m^2$). Comparison with the results for a model of high-ohmic lithosphere (see Figures 2c and 2d) supports one of the

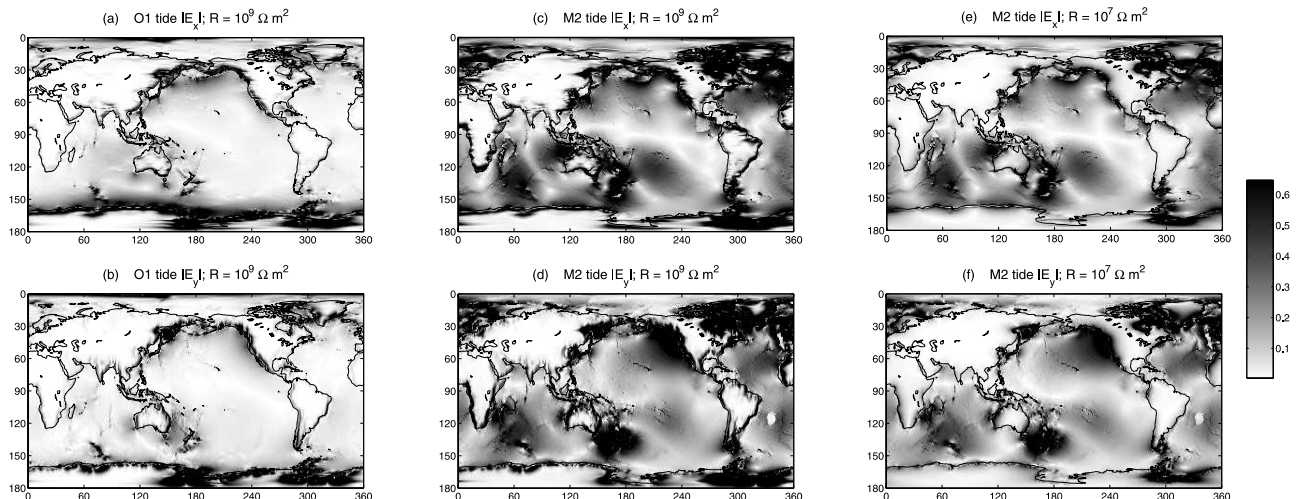


Figure 2. (a)–(d) Amplitudes of electric field (mV/km) due to O1 and M2 tides for the model with $R = 10^9 \Omega m^2$. (e)–(f) M2 tide electric field for the model with $R = 10^7 \Omega m^2$ (see details in the text).

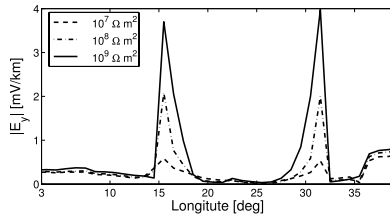


Figure 3. Amplitudes of M2 tide E_y along $30^\circ S$ profile that crosses South Africa, for different values of R . The longitudinal location of the coasts are $15.5^\circ E$ and $31.5^\circ E$.

significant features of the motionally-induced electric field [cf. *Palshin et al. 1999*] - its dependence on R . The model with a resistive lithosphere shows coastal anomalies which are much more prominent in amplitudes and decay at larger distances inland, as a result of smaller leakage effect. Figure 3 illustrates the tidal electric field dependence on R in more detail. It presents, for different values of R , amplitudes of the west-east component of the M2 tide electric field along a $30^\circ S$ profile that crosses South Africa. Coastal tidal signal varies here from 0.5 mV/km for $R = 10^7 \Omega m^2$ to 4 mV/km for $R = 10^9 \Omega m^2$.

4. Comparison With Observations

[8] Next we compare our predictions with the M2 tide electric signals which were observed by *Junge* [1988] at four sites in northern Germany [cf. *Junge*, 1988, Table 1]. Figure 4 presents the results of comparison. Location of the sites is shown in Figure 5a. Overall, the predicted amplitudes (solid curves as a functions of $\log_{10} R$) are in a quite good agreement with the observed amplitudes (dashed straight lines). The discrepancy is put down to local inhomogeneities of the near-surface conductivities. Thus the comparison between observed and modeled data could give important information about the distortion of the electrical field due to the lateral conductivity distribution. Note, that for these comparisons we use the Earth's model of *Schmucker* [1985] as the underlying 1-D conductor, since it provides better agreement between predictions and observations. Also Figure 4 demonstrates quantitatively the sensitivity of the predicted electric signals to R . As an example, the two order change in R leads to the one order change in amplitude of E_x at site Deppoldshausen (DEP). Another interesting result is that there is such a large difference between the electric fields at four closely situated stations both in the predictions and observations. Figure 5 allows the reader to see what is going on in this region. Figure 5 presents amplitudes of (a) E_x (which is dominant component for the sites considered), (b) U_y (which is mainly responsible for E_x ; see equation (1)), and (c) the regional S , respectively. It is seen that indeed the electric field strongly varies within the region and such a variability is consistent with the conductance and velocity distributions. For example, large sediments in northern Germany weaken here tidal electric field. Conversely, contrast in conductance produces relatively large signal in the central part of Germany. Lastly, it is relevant to mention, that the phases of predicted electric signals (not shown here) also agree well with the experimental ones, but, as expected, are less influenced by R .

[9] Figure 6 demonstrates, in a similar manner, the comparison between predicted voltages due to M2 and O1 tides and the experimental voltages which were derived by *Fujii and Utada* [2000] at four northern Pacific Ocean cables [cf. *Fujii and Utada*, 2000, Table 3]. The location of the cables is shown in Figure 6 (right). It is seen that for the voltages the agreement between predictions and observations are better than for inland electric field (see Figure 4), especially for M2 tide results. Possible explanation of this fact is that the ocean conductance - major controlling parameter for cable voltages - is better known than the land conductance and that the voltages are taken over a rather long distance thus averaging out the influence of lateral conductivity inhomogeneities. It is also seen that the voltage predictions don't reveal pronounced dependence on R . The largest changes are detected for M2 tide voltage at Philippine-Guam (P2G) cable, where the two order change in R leads to double change in the predicted signal. Weak dependence of the voltage on R is not surprising, since the maximum effect due to the changes of R is observed in the electric signals at the sharp lateral contrast of conductivity, which, however, enter as a small portion in the total voltages from the considered long submarine cables. In spite of this fact one can see that as a whole the best agreement between predictions and observations is achieved when R lies in the range of $10^8 \Omega m^2$ and $10^9 \Omega m^2$ which is consistent with previous R estimates for this region [*Utada et al.*, 2003].

5. Conclusions

[10] Our numerical simulations provide estimations of the electric fields generated by ocean tides and reveal the regions most favourable to detect and to study these fields. Maximum tidal signals are observed on the coasts where they can reach 10 mV/km and 100 mV/km for respective O1 and M2 tides. Simulations clearly demonstrate the significant feature of motionally-induced electric field - its dependency on lithosphere resistance. On average two order change in resistance leads to one order change in the coastal electric signal.

[11] The predictions as a whole are in a good agreement with experimental tidal electric signals from the northern

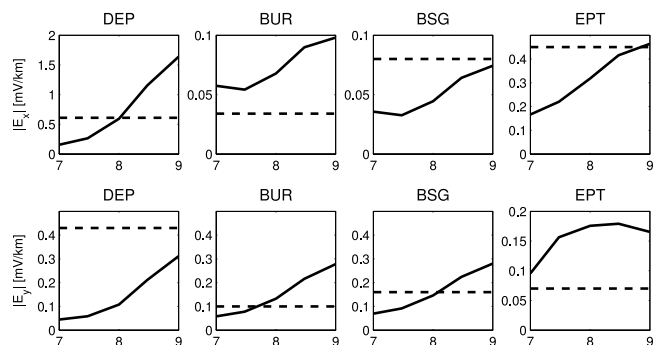


Figure 4. Predicted amplitudes (solid curves as a functions of $\log_{10} R$) and observed amplitudes (dashed straight lines) of M2 tide electric field in northern Germany. The upper and lower rows show the results for E_x and E_y components, respectively.

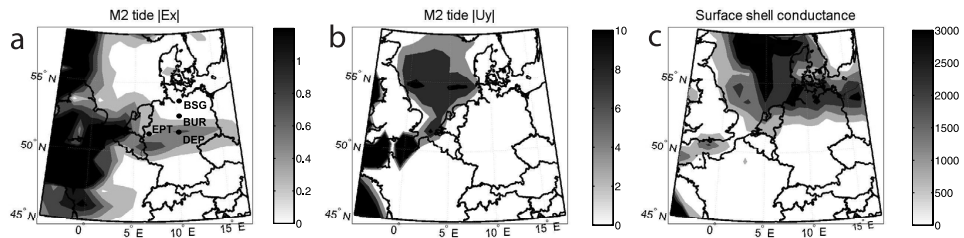


Figure 5. Amplitudes of (a) E_x (mV/km), (b) U_y (m^2/s), and (c) conductances (S) in western Europe. Electric field is calculated for the model with $R = 10^8 \Omega m^2$.

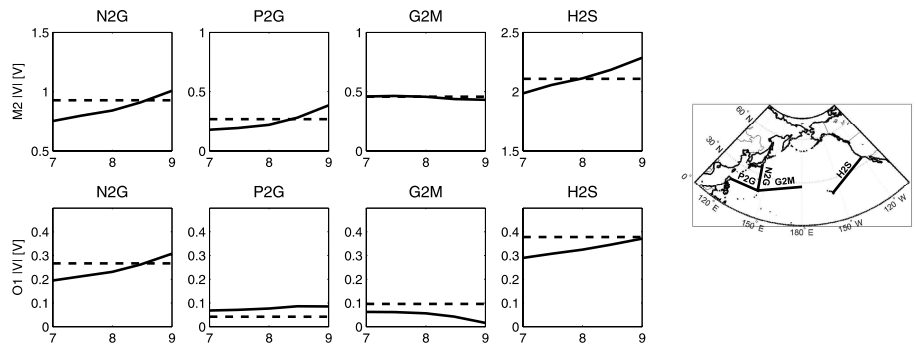


Figure 6. Predicted amplitudes (solid curves as a functions of $\log_{10} R$) and observed amplitudes (dashed straight lines) of tidal voltages, V , from northern Pacific Ocean cables. The results for (top) M2 and (bottom) O1 tides, respectively.

Germany sites and tidal voltage signals from the northern Pacific Ocean cables. An agreement is especially encouraging for the cable data and suggests lithosphere resistance in the range of $10^8 \Omega m^2$ and $10^9 \Omega m^2$. However some discrepancy still exists for the northern Germany data. It would motivate further investigations, which might include, say, improvements in the Earth's conductivity or/and tidal models. Present model predictions are available at anonymous ftp-server ftp.spacecenter.dk/data/tides/E-field.

References

- Duffus, H. J., and N. R. Fowler (1974), On planetary voltages, ocean tides, and electrical conductivity below the Pacific, *Can. J. Earth Sci.*, *11*, 873–892.
- Erofeeva, S., and G. Egbert (2002), Efficient inverse modelling of barotropic ocean tides, *J. Atmos. Oceanic Technol.*, *19*, 183–204.
- Flosadottir, A., J. Larsen, and J. Smith (1997), Large-scale electric and magnetic fields generated by the oceans, *J. Geophys. Res.*, *102*, 10,353–10,372.
- Fujii, I., and H. Utada (2000), On geoelectric potential variations over a planetary scale, *Mem. Kakioka Magn. Obs.*, *29*, 1–71.
- Harvey, R. R., J. C. Larsen, and R. Montaner (1977), Electric field recording of tidal currents in the Strait of Magellan, *J. Geophys. Res.*, *82*, 3472–3476.
- Junge, A. (1988), The telluric field in northern Germany induced by tidal motion in North Sea, *Geophys. J. Int.*, *95*, 523–533.
- Kuvshinov, A., and N. Olsen (2005), 3-D modelling of the magnetic fields due to ocean tidal flow, in *Earth Observation with CHAMP: Results From Three Years in Orbit*, edited by C. Reigber et al., pp. 359–366, Springer, New York.
- Kuvshinov, A. V., D. B. Avdeev, O. V. Pankratov, S. A. Golyshev, and N. Olsen (2002), Modelling electromagnetic fields in 3D spherical Earth using fast integral equation approach, in *3D Electromagnetics*, edited by M. S. Zhdanov and P. E. Wannamaker, chap. 3, pp. 43–54, Elsevier, New York.
- Kuvshinov, A. V., H. Utada, D. Avdeev, and T. Koyama (2005), 3-D modelling and analysis of Dst C-responses in the North Pacific Ocean region, revisited, *Geophys. J. Int.*, *160*, 505–526.
- Laske, G., and G. Masters (1997), A global digital map of sediment thickness, *Eos Trans. AGU*, *78*(17), Fall Meet. Suppl., F483.
- Manoj, C., A. Kuvshinov, S. Maus, and H. Lühr (2006), Ocean circulation generated magnetic signals, *Earth Planets Space*, in press.
- Maus, S., and A. Kuvshinov (2004), Ocean tidal signals in observatory and satellite magnetic measurements, *Geophys. Res. Lett.*, *31*, L15313, doi:10.1029/2004GL020090.
- Palshin, N. A., L. L. Vanyan, I. V. Yegorov, and K. V. Lebedev (1999), Electric fields induced by the global ocean circulation, *Phys. Solid Earth*, *35*, 1028–1035.
- Rooney, W. J. (1938), Lunar diurnal variation in Earth currents at Huancayo and Tucson, *J. Geophys. Res.*, *43*, 107–118.
- Schmucker, U. (1985), Electrical properties of the Earth's interior, in *Geophysics of the Solid Earth, the Moon and the Planets, Landolt-Börnstein Group V Geophys.*, vol. 2B, pp. 370–397, Springer, New York.
- Stephenson, D., and K. Bryan (1992), Large-scale electric and magnetic fields generated by the oceans, *J. Geophys. Res.*, *97*, 15,467–15,480.
- Tyler, R., J. Oberhuber, and T. Sanford (1999), The potential for using ocean generated electromagnetic field to remotely sense ocean variability, *Phys. Chem. Earth A*, *24*, 429–432.
- Tyler, R., S. Maus, and H. Lühr (2003), Satellite observations of magnetic fields due to ocean tidal flow, *Science*, *299*, 239–241.
- Utada, H., T. Koyama, H. Shimizu, and A. D. Chave (2003), A semi-global reference model for electrical conductivity in the mid-mantle beneath the north Pacific region, *Geophys. Res. Lett.*, *30*(4), 1194, doi:10.1029/2002GL016092.
- Vivier, F., E. Maier-Reimer, and R. H. Tyler (2004), Simulations of magnetic fields generated by the Antarctic Circumpolar Current at satellite altitude: Can geomagnetic measurements be used to monitor the flow?, *Geophys. Res. Lett.*, *31*, L10306, doi:10.1029/2004GL019804.

A. Junge, Institute of Meteorology and Geophysics, University of Frankfurt am Main, Feldberstrasse 47, D-60323 Frankfurt am Main, Germany.

A. Kuvshinov, Danish National Space Center, Juliane Maries Vej 30, DK-2100 Copenhagen, Denmark. (alexei@spacecenter.dk)

H. Utada, Ocean Hemisphere Research Center, Earthquake Research Institute, University of Tokyo, Tokyo 113-0032, Japan.